MECH0064 MSc Group Design Project

Compact Continuum Robotic Manipulator Platform

Group members:

Zehao Ye (23119333) Yuhao Zhu (23041703)

Zehao Ye (23119333) Zehao Ye (23119333)

Zehao Ye (23119333) Zehao Ye (23119333)

Supervised by Dr Reza Haqshenas

Abstract

This is the Abstract of the final report.

AAAAA bbb

test for github

Key Words: Continuum Robotic e.g.

Contents

List of Figures

List of Tables

1 Introduction

1.1 Background

This is the background part.

1.2 Motivation

This is the motivation part.

1.3 Introduction

Continuum robots has emerged and attracted a lot of attention since 2008 [1]. Before that, rigid joint robots were dominating the robotic arm industry. Compared with traditional rigid joint manipulator, continuum robots stand out for their flexible, highly bendable structure and extremely flexible motion performance. The limitations of rigid joint robots have gradually shown up in applications requiring highly detailed operation and in complex or space-limited environments. Thus, the continuum robot was developed and perfected during the years. This new kind of robot not only changes the code of traditional robot design but also demonstrates unprecedented application potential in fields such as exploration industry and medical science [2]. Meanwhile, rigid-flexible-soft coupled continuum robots combine the multiple advantages of the stability of rigid structures, the flexibility of bendable structures, and the compliance of soft structures, and are one of the most promising robots for increasingly complex tasks [3].

With unique bionic structure and motion characteristics, continuum robots provide new possibilities to solve these challenges.

This paper will discuss different types of existing continuum robots and their working principles, advantages, and disadvantages, then propose a proper continuum robot design that can be mainly applied to medical applications.

2   Literature Review

In the last two decades, significant progress in electronic and computer technologies has led to remarkable growth in the field of manipulator robotics. Manipulators developed by various institutions have been integrated into the industrial sector to autonomously or semi-autonomously perform repetitive tasks. Simultaneously, manipulators are utilized for tasks with stringent precision requirements to minimize errors. Additionally, essential tasks are undertook by manipulators to substitute for humans in challenging environments.

2.1   Manipulators in Biology Field

With a growing emphasis on the field of biology, manipulators have also been introduced to provide assistance. In the field of medicine, manipulators have been utilized since the end of the last century. The AESOP robotic surgical system, proposed by Computer Motion founded by Yulun Wang in 1993, was investigated in laparoscopic surgery in 1997 [4]. Afterward, the ZEUS robotic surgical system endowed with a trilateral manipulator configuration was proposed by Computer Motion in 1998 [5].During the period from 1999 to 2001, the ZEUS system was utilized for a series of clinical surgeries, demonstrating excellent performance [6–8]. At the beginning of the 21st century, a novel robotic system, da Vinci robotic surgery system, was designed to facilitate more intricate surgical procedures [9]. Moreover, manipulators can be leveraged in the field of biological physics as a viable approach for biological experiments. In the HIFU system developed by An et al., the SCARA (self compliant automatic robot assembly) robot was employed as manipulator, incorporating an ultrasound probe for the purpose of scanning biological tissues [10]. The robotic system FUSBOTs (Focal Ultrasound Surgery RoBOTs) was proposed and upgraded to accomplish more precise targeted treatment with multiple DoF (Degrees of Freedom) manipulators [11–13]. Despite the various utilization of manipulator platforms designed for accommodating ultrasonic transducers [14–16], certain limitations persist. Hence, a comparison of different manipulators is necessary in selection of appropriate type manipulator for integrating ultrasonic transducer.

2.2 Types of Manipulator

From the perspective of geometry, rigid-body manipulators can be categorized into two main types: parallel mechanisms and serial link [17]. The control of parallel mechanisms is relatively complex. Meanwhile, serial link manipulators can be further divided into five types: Cartesian (PPP), articulated (RRR), cylindrical (RPP), spherical (RRP), and SCARA (RRP). Additionally, with the advancement of robotics technology, two other types of manipulators, namely biomimetic and anthropomorphic, have demonstrated their advantages [18, 19]. The comparative analysis will be conducted to highlight the distinctive features of different manipulators presented in Table 1, leading to the identification of the most suitable type for specific applications.

Table 1: The Characteristics of Different Manipulators.

Manipulators	Types	DoF	Features	Applications
Stewart Platform [20]	Series-Parallel	6	series-parallel duality, mature kinematics algorithm.	flight simulation [21]. robocrane [22]
Cartesian	PPP	3	technological maturity, low complexity, cost-effective, high payload.	3D-Printing framework [23] warehousing & hoisting [24] agricultural machinery [25]
Articulated [26]	RRR	6	factory automation, programmable, high precision and payload.	milling operations [27] material handling [28]
Cylindrical [29]	RPP	3	good precision, limited workspace.	assembling industries [30]
Spherical [31]	RRP	3	collision avoidance, low precision, long reach, light weight.	low-precision semi-automated tasks [27, 28]
SCARA [29]	RRP	3	high accuracy and fast operation.	surgical applications [32] medical rehabilitation [33]
Continuum/ Soft [34, 35]	Biomimetic	∞	ability to handle fatigue objects, environmental adaptability.	tendon driven [36–38] fibre-reinforced [39, 40] fluid-elastic drive [41–43] bionics materials [44–46]

Table 1 – continued from previous page

Manipulators	Types	DoF	Features	Applications
Humanoid	anthropo-morphic	7	high efficiency, flexibility.	humanoid robots driven by pneumatic artificial muscles [47]

The distinctive structure of continuum manipulator imparts to the system with theoretically infinite DoF. The characteristic enables the continuum manipulator to navigate through confined spaces or manipulate objects along specific trajectories within the workspace [2, 34, 35]. Simultaneously, the continuum maniuplator demonstrates suboptimal performance in the context of payload, making it challenging to meet the payload capacities commonly observed in industrial robotic systems. Nevertheless, within the realm of biology applications, the emphasis shifts towards precision and operability for manipulator. In this report, the manipulator platform integrated with the ultrasonic transducer module necessitates a design. The selection of the continuum manipulator was predicated upon its outstanding flexibility and the lightweight attributes of ultrasonic transducer module. The forthcoming discussion will delve into the categorisation of continuum robots, ultimately selecting an appropriate type to serve as the centerpiece for the manipulator platform.

2.3 Types of Continuum Robots

Nowadays, a variety of continuum robots exist, each exhibiting unique structures and functions. They serve in different fields such as medicine, construction, and exploration. In this section, some of the most popular continuum robots will be introduced, providing basic insights into their structures as well as discussing their merits and drawbacks.

2.3.1 Tendon-Driven Robots

The arm of the Tendon-Driven robot consists of a backbone, several tendons and disks. The backbone defines the structure and posture of the entire robot arm, while disks

define the diameter and divide the robot arm into segments, and tendons are stretched to create deformation and movements of different directions for the robot arm.
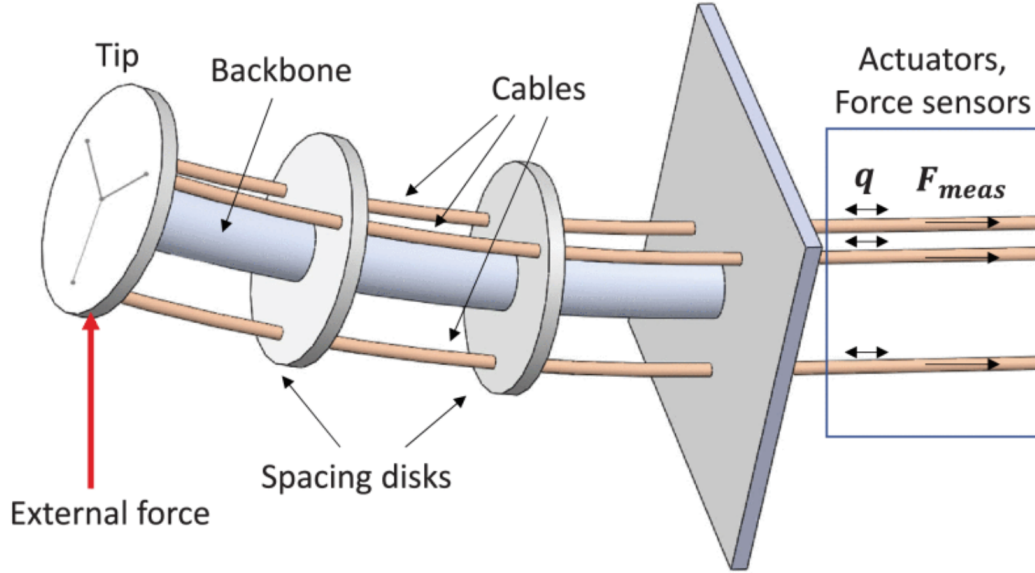
Figure 1: *The three tendons continuum robot with one segment* [48].

Figure 1 shows only the simplest tenon-driven robots. In practical applications, there may be more than one backbone, and the disks are not necessarily parallel.

Compared with other continuum robots, one of the most significant advantages of tendon-driven robots is their flexibility. This advantage makes it more effective in performing tasks in complex and restrictive Spaces. In addition, due to the simple components needed to construct the robot, it is easier to meet lightweight design specifications. Moreover, like the concentric-tube continuum robots, tendon-driven continuum robots can be built designed on a small scale with diameters of below 10mm [49].

However, due to its simple actuating principle, more complex algorithms are needed to control it more accurately. Also, the tendon-driven robots actuate by pulling the tendon, which makes the friction between the tendon and other components inevitable, which will accelerate the wearing speed of the tendon-driven robots.

2.3.2   Fishbone Robots

Fishbone robots, as the name suggests, are inspired by fish bones. It is consists of several "fishbone moduless", which are composed of a number of rigid cross-shaped plates, and a flexible elastic plate backbone embedded in the middle, forming a rigid-soft coupling

structure[3]. When the different modules are connected, the backbones of the bionic fishbone modules are perpendicular to each other, and finally form a complete main frame of the fishbone robot. Like the tendon-driven robot, the fishbone robot is also controlled by cable, but it is worth noting that each module is controlled by two separate cables. This means that for a fishbone robot composed of n fishbone modules, there are a total of 2n cables controlling the motion of the whole robot. In addition, the planes formed by the two ropes that control each module are perpendicular to each other, so that each section rotates along a plane perpendicular to each other.
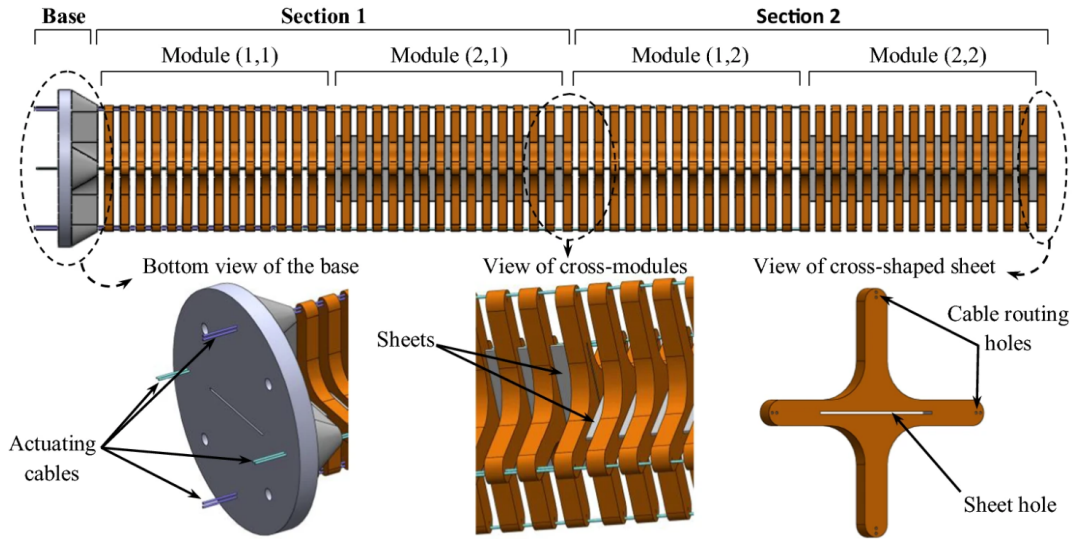
**Figure 2:** *The cable-driven fish bone continuum robot with cable arrangement* [50].

From the graph above, it is shown that because of the numbers of rigid cross-shaped sheets formed a large diamater frame, the structural stability of this kind of robot is very strong. Also, each fishbone unit can provide one DoF, making it easy to reach a very high total DoF. However, due to the multiple-curves deformation trajectory, the fishbone robots are not suitable for situations where strict trajectory is required[3].

2.3.3   Concentric Tube Continuum Robots

concentric tube robots, shaped like retractable walking sticks, consist of many tubes with decreasing diameters. Each tube is nested on top of the previous wider tube.
The concentric robots are made of two parts: tubes and coaxial actuation units. The tubes are the main structural element of this robot and act as the backbone. The coaxial

actuation unit consists of two motors which are responsible for rotation and translation movement respectively. Each tube is actuated by an independent coaxial actuation unit.
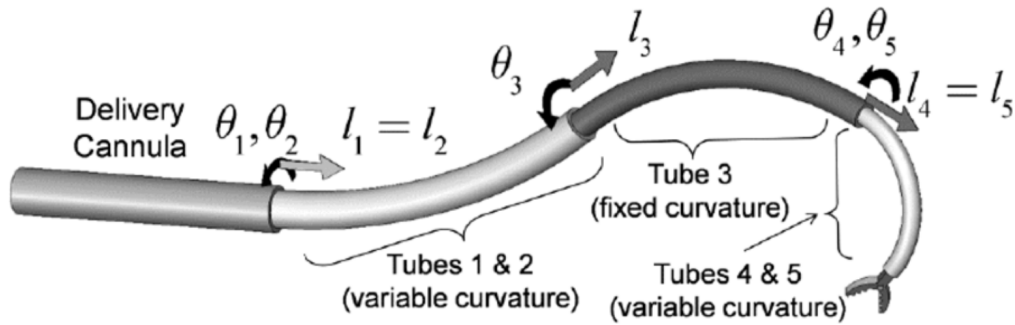
Figure 3: *An example concentric tube continuum robot* [51].

The most significant advantage of this kind of robots is that of all the continuum robots, concentric tube robots have the smallest possible outer diameter and are best suited to work in confined and narrow Spaces. Therefore, it is the ideal choice for surgical operations.

Their disadvantages, on the other hand, are also very evident. Since each tube requires an independent actuation unit, the overall length of the robot cannot be very long, because longer lengths will lead to more tubes, and will lead to more tip position errors.

3 Design

This is the Design of the final report.

3.1 Working Principles

Continuum robot can be broadly divided into two parts: a continuous bending structure and a fixed base containing actuating and controlling devices.

The continuous bending structure can be seen as the working arm of the robot. A flexible backbone shapes the arm, and it can be rotated and bent by dragging/releasing the different cables (tendons) around it. When the joystick in the fixed base is manipulated manually, the programmed stepper motor will step forward/backward by the corresponding number of steps. These motors are connected to different cables located in the bending structure (arm), the motors dragging the cables, thereby making cable contract. Finally, the contraction of different cables will rotate and bend the backbone, which is the core component of the arm, thereby changing the posture of the arm.

This process can be likened to the movement of the human arms. cables can be understood as tendons/muscle bundles and backbone as the main skeleton.

Figure 4: *An example of continuum robot* [52].

Different types of continuum robots have different backbones, actuating and flexible components, but they are generally all work under the same working principle stated above.

3.2 Methodology

3.2.1 Forward Kinematics

The manipulator consists of four units, and the backbones of each section are perpendicular to each other. To derive the workspace of the manipulator for further analysis, the forward kinematics formula need to be conducted. According to the fishbone continuum robot[3], the forward kinematics formula of two perpendicular units

are shown in Equations 1, 2, and 3.

$$x = -\frac{S_r r}{\Delta S_1} + \frac{S_r r}{\Delta S_1} \cos\left(\frac{\Delta S_l}{r}\right) - d_1 \sin\left(\frac{\Delta S_l}{r}\right)$$
$$- \frac{S_r r}{\Delta S_3} \sin\left(\frac{\Delta S_1}{r}\right) \sin\left(\frac{\Delta S_3}{r}\right) - d_2 \sin\left(\frac{\Delta S_1}{r}\right) \cos\left(\frac{\Delta S_3}{r}\right) \tag{1}$$

$$y = -\frac{S_r r}{\Delta S_3} + \frac{S_r r}{\Delta S_3} \cos\left(\frac{\Delta S_3}{r}\right) - d_2 \sin\left(\frac{\Delta S_3}{r}\right) \tag{2}$$

$$z = \frac{S_r r}{\Delta S_1} \sin\left(\frac{\Delta S_1}{r}\right) + d_1 \cos\left(\frac{\Delta S_1}{r}\right)$$
$$+ \frac{S_r r}{\Delta S_3} \sin\left(\frac{\Delta S_3}{r}\right) \cos\left(\frac{\Delta S_1}{r}\right) + d_2 \cos\left(\frac{\Delta S_1}{r}\right) \cos\left(\frac{\Delta S_3}{r}\right). \tag{3}$$

However, calculating the centroid directly using the above formula becomes complex while there are four units in the manipulator. Additionally, the inverse kinematics part also requires the derivation of corresponding matrices for subsequent calculations using the composite coordinate transformation formula. Therefore, The relevant matrices for subsequent calculations need to be derived.

According to the design specifications, the manipulator comprises four units. The backbones of the units are vertically aligned. The base coordinate system can be established with the centroid of base disk upper surface serving as the origin. The x-axis of the coordinate system is aligned with the backbone of the unit nearest to the base disk. Consequently, the backbones of units 1 and 3 are parallel to the x-axis, while those of units 2 and 4 are parallel to the y-axis. The positions of the five centroids in the base coordinate system when the manipulator is in the initial position are shown in Figure 5. The centroids of the five disc upper surfaces are designated as $node_1$, $node_2$, $node_3$, $node_4$, and $node_5$.
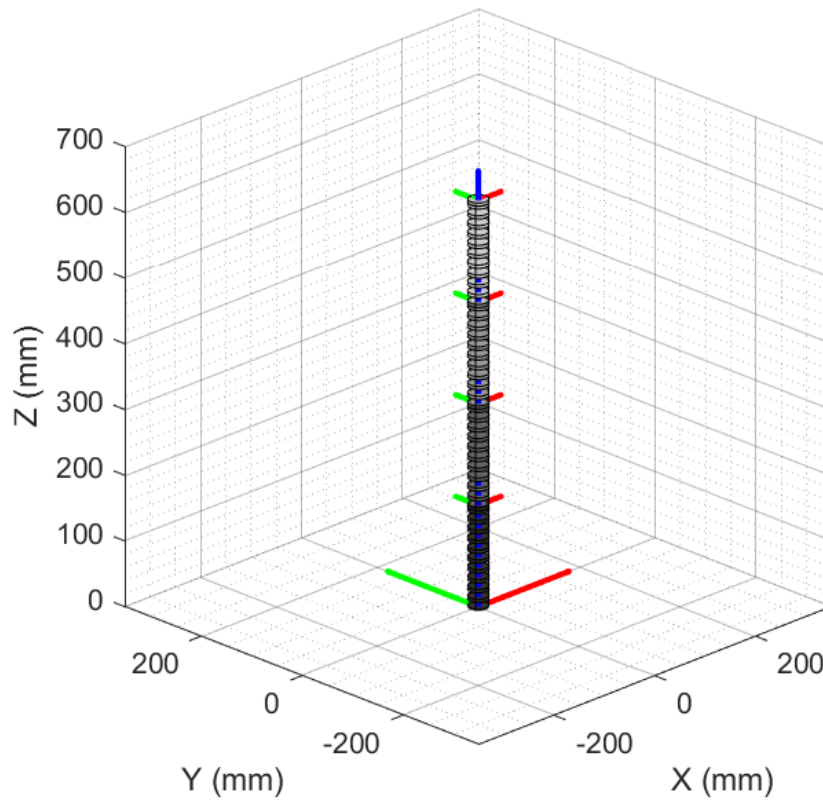
Figure 5: *The kinematics model of manipulator in initial position.*

The unit 1 is restricted to bending in the y-z plane of the coordinate system where $node_1$ serves as the origin, while the unit 2 is restricted to bending in the x-z plane of the coordinate system where $node_2$ serves as the origin. Similarly, the unit 3 and unit 4 are subject to the same constraints. The bending angles for these units are defined as α_1, α_2, α_3, and α_4, respectively. The positions of the manipulator model in the base coordinate system after bending each unit by 90° are illustrated in Figure 6.
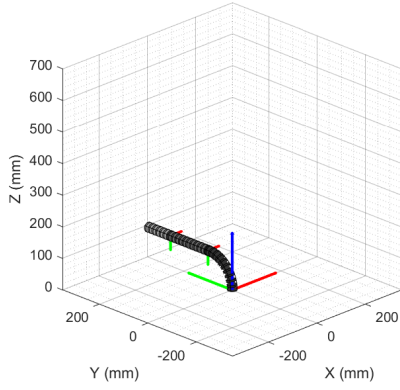
(a) $\alpha_1 = 90°, \alpha_2 = 0, \alpha_3 = 0, \alpha_4 = 0$
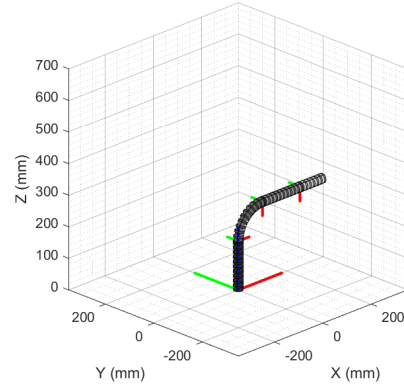
(b) $\alpha_1 = 0, \alpha_2 = 90°, \alpha_3 = 0, \alpha_4 = 0$
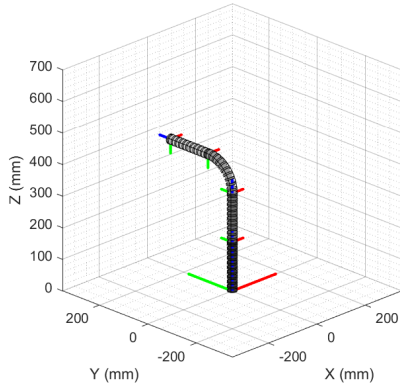
(c) $\alpha_1 = 0, \alpha_2 = 0, \alpha_3 = 90°, \alpha_4 = 0$
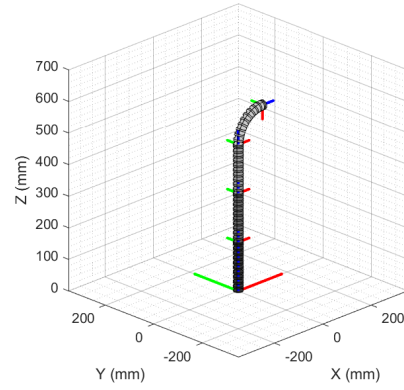
(d) $\alpha_1 = 0, \alpha_2 = 0, \alpha_3 = 0, \alpha_4 = 90°$

Figure 6: *The kinematics model of manipulator with respective bending units.*

While the units bend to the positive direction of x-axis or y-axis, the bending angles α are positive. Owing to the distinct properties of the four units, different calculation methods are required for analysis. The unit i have a base node $node_i$ and an end effector node $node_{i+1}$. To further calculate the position of $node_{i+1}$ in the base coordinate system, these matrices can be employed in the Equation 4.

$$\mathbf{P}_{i+1}^{base} = \mathbf{R}_i \times \mathbf{P}_{i+1}^{i} + \mathbf{P}_{i}^{base} \tag{4}$$

$\mathbf{P}_{i+1}^{base}$: The position of $node_{i+1}$ in the base coordinate system.

$\mathbf{R}_i$: The rotational matrix tranforms the base coordinate system into coordinate system i, which is the coordinate system with origin $node_i$.

$\mathbf{P}_{i+1}^{i}$: The position of $node_{i+1}$ in coordinate system i.

$\mathbf{P}_i^{base}$: The position of $node_i$ in the base coordinate system.

- Unit 1

  For Unit 1, the relationship between the relative position matrix of $node_1$ and $node_2$ $\mathbf{P}_2^1$ and α_1 is shown in Equation 5.

$$\mathbf{P}_2^1 = \begin{bmatrix} 0 \\ (R_1 \cdot (1 - \cos(\alpha_1)) + d_2 \cdot \sin(\alpha_1)) \\ (R_1 \cdot \sin(\alpha_1) + d_2 \cdot \cos(\alpha_1)) \end{bmatrix} \tag{5}$$

$$(hint: \ R_1 = Sr_1/\alpha_1)$$

  R_1 is the radius of the Unit 1 bending curve, Sr_1 is the length of the Unit 1 backbone, and d_2 is the thickness of the disc whose centroid is $node_2$. Meanwhile, the rotational matrix $\mathbf{R}_1$ and the position matrix of $node_1$ $\mathbf{P}_1^{base}$ are shown in Equations 6 and 7.

$$\mathbf{R}_1 = \begin{bmatrix} 1 & 0 & 0 \\ 0 & 1 & 0 \\ 0 & 0 & 1 \end{bmatrix} \tag{6}$$

$$\mathbf{P}_1^{base} = \begin{bmatrix} 0 & 0 & 0 \end{bmatrix}^{\mathbf{T}} \tag{7}$$

  According to the Equations 5, 6, and 7, the position matrix of $node_2$ in the base coordinate system $\mathbf{P}_2^{base}$ can be calculated in Equation 8.

$$\begin{aligned} \mathbf{P}_2^{base} &= \mathbf{R}_1 \times \mathbf{P}_2^1 + \mathbf{P}_1^{base} \\ &= \begin{bmatrix} 1 & 0 & 0 \\ 0 & 1 & 0 \\ 0 & 0 & 1 \end{bmatrix} \times \begin{bmatrix} 0 \\ (R_1 \cdot (1 - \cos(\alpha_1)) + d_2 \cdot \sin(\alpha_1)) \\ (R_1 \cdot \sin(\alpha_1) + d_2 \cdot \cos(\alpha_1)) \end{bmatrix} + \begin{bmatrix} 0 \\ 0 \\ 0 \end{bmatrix} \\ &= \begin{bmatrix} 0 \\ (R_1 \cdot (1 - \cos(\alpha_1)) + d_2 \cdot \sin(\alpha_1)) \\ (R_1 \cdot \sin(\alpha_1) + d_2 \cdot \cos(\alpha_1)) \end{bmatrix} \end{aligned} \tag{8}$$

- Unit 2

  For Unit 2, the relationship between the relative position matrix of $node_2$ and $node_3$

$\mathbf{P}_3^2$ and α_2 is shown in Equation 9.

$$\mathbf{P}_3^2 = \begin{bmatrix} (R_2 \cdot (1 - \cos(\alpha_2)) + d_3 \cdot \sin(\alpha_2)) \\ 0 \\ (R_2 \cdot \sin(\alpha_2) + d_3 \cdot \cos(\alpha_2)) \end{bmatrix} \tag{9}$$

$$(hint: \ R_2 = Sr_2/\alpha_2)$$

R_2 is the radius of the Unit 2 bending curve, Sr_2 is the length of the Unit 2 backbone, and d_3 is the thickness of the disc whose centroid is $node_3$. Meanwhile, the rotational matrix $\mathbf{R}_2$ and the position matrix of $node_2$ $\mathbf{P}_2^{base}$ are shown in Equations 10 and 8.

$$\mathbf{R}_2 = \begin{bmatrix} 1 & 0 & 0 \\ 0 & \cos(\alpha_1) & \sin(\alpha_1) \\ 0 & -\sin(\alpha_1) & \cos(\alpha_1) \end{bmatrix} \tag{10}$$

According to the Equations 8, 9, and 10, the position matrix of $node_3$ in the base coordinate system $\mathbf{P}_3^{base}$ can be calculated in Equation 11.

$$\mathbf{P}_3^{base} = \mathbf{R}_1 \times \mathbf{R}_2 \times \mathbf{P}_3^2 + \mathbf{P}_2^{base}$$

$$= \begin{bmatrix} 1 & 0 & 0 \\ 0 & 1 & 0 \\ 0 & 0 & 1 \end{bmatrix} \times \begin{bmatrix} 1 & 0 & 0 \\ 0 & \cos(\alpha_1) & \sin(\alpha_1) \\ 0 & -\sin(\alpha_1) & \cos(\alpha_1) \end{bmatrix}$$

$$\times \begin{bmatrix} (R_2 \cdot (1 - \cos(\alpha_2)) + d_3 \cdot \sin(\alpha_2)) \\ 0 \\ (R_2 \cdot \sin(\alpha_2) + d_3 \cdot \cos(\alpha_2)) \end{bmatrix}$$

$$+ \begin{bmatrix} 0 \\ (R_1 \cdot (1 - \cos(\alpha_1)) + d_2 \cdot \sin(\alpha_1)) \\ (R_1 \cdot \sin(\alpha_1) + d_2 \cdot \cos(\alpha_1)) \end{bmatrix} \tag{11}$$

- Unit 3

For Unit 3, the relationship between the relative position matrix of $node_3$ and $node_4$

$\mathbf{P}_4^3$ and α_3 is shown in Equation 12.

$$\mathbf{P}_4^3 = \begin{bmatrix} 0 \\ (R_3 \cdot (1 - \cos(\alpha_3)) + d_4 \cdot \sin(\alpha_3)) \\ (R_3 \cdot \sin(\alpha_3) + d_4 \cdot \cos(\alpha_3)) \end{bmatrix} \tag{12}$$

$$(hint: \ R_2 = Sr_2/\alpha_2)$$

R_3 is the radius of the Unit 3 bending curve, Sr_3 is the length of the Unit 3 backbone, and d_4 is the thickness of the disc whose centroid is $node_4$. Meanwhile, the rotational matrix $\mathbf{R}_3$ and the position matrix of $node_3$ $\mathbf{P}_3^{base}$ are shown in Equations 13 and 11.

$$\mathbf{R}_3 = \begin{bmatrix} \cos(\alpha_2) & 0 & \sin(\alpha_2) \\ 0 & 1 & 0 \\ -\sin(\alpha_2) & 0 & \cos(\alpha_2) \end{bmatrix} \tag{13}$$

According to the Equations 11, 12, and 13, the position matrix of $node_4$ in the base coordinate system $\mathbf{P}_4^{base}$ can be calculated in Equation 14.

$$\mathbf{P}_4^{base} = \mathbf{R}_1 \times \mathbf{R}_2 \times \mathbf{R}_3 \times \mathbf{P}_4^3 + \mathbf{P}_3^{base}$$

$$= \mathbf{R}_1 \times \mathbf{R}_2 \times \begin{bmatrix} \cos(\alpha_2) & 0 & \sin(\alpha_2) \\ 0 & 1 & 0 \\ -\sin(\alpha_2) & 0 & \cos(\alpha_2) \end{bmatrix}$$

$$\times \begin{bmatrix} 0 \\ (R_3 \cdot (1 - \cos(\alpha_3)) + d_4 \cdot \sin(\alpha_3)) \\ (R_3 \cdot \sin(\alpha_3) + d_4 \cdot \cos(\alpha_3)) \end{bmatrix} + \mathbf{P}_3^{base} \tag{14}$$

- Unit 4

  In summary, the position matrix of $node_5$ in the base coordinate system P_5^{base} can be represented by Equation 15.

$$\mathbf{P}_5^{base} = \mathbf{R}_1 \times \mathbf{R}_2 \times \mathbf{R}_3 \times \mathbf{R}_4 \times \mathbf{P}_5^4 + \mathbf{P}_4^{base} \tag{15}$$

Applying the corresponding transformations to the Equation 4 reveals the patterns

shown in Equations 16 and 17.

$$\mathbf{P}_{i+1}^{base} - \mathbf{P}_{i}^{base} = \prod_{n=1}^{i} \mathbf{R}_n \times \mathbf{P}_{i+1}^{i} \tag{16}$$

$$\mathbf{P}_{i+1}^{base} = \sum_{m=1}^{i} \left[\prod_{n=1}^{m} \mathbf{R}_n \times \mathbf{P}_{m+1}^{m} \right] \quad (\mathbf{P}_{1}^{base} = 0) \tag{17}$$
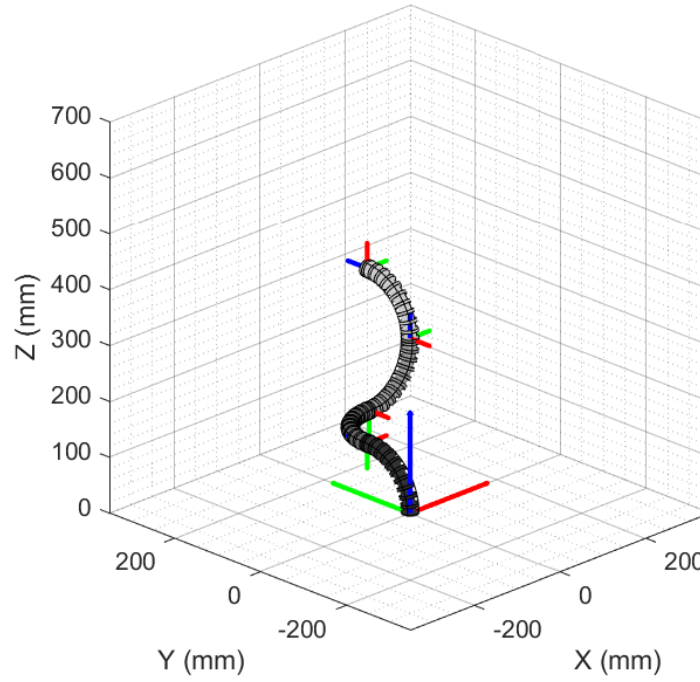
(a) $\alpha_1 = 90°, \alpha_2 = 90°, \alpha_3 = -90°, \alpha_4 = -90°$
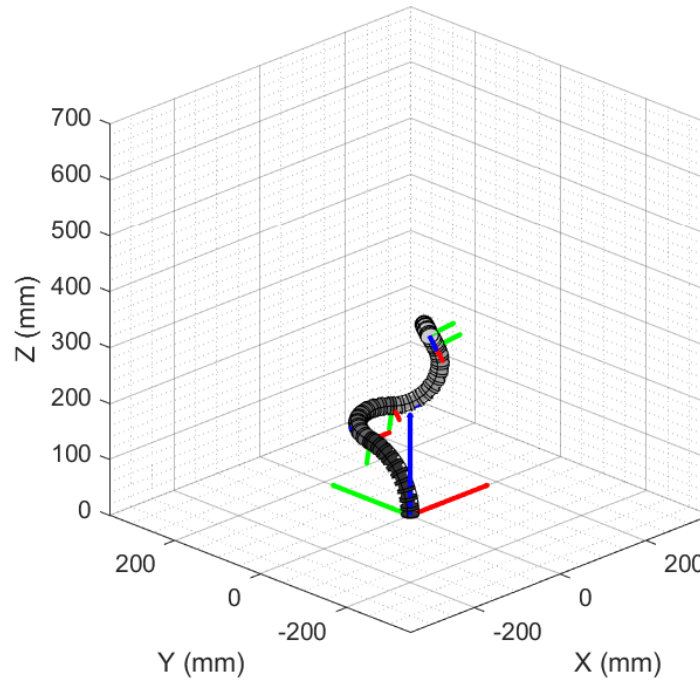
(b) $\alpha_1 = 80°, \alpha_2 = 120°, \alpha_3 = -120°, \alpha_4 = 90°$

Figure 7: *The kinematics model of manipulator with respective bending units.*

To emphasize transformation of manipulator, homogeneous transformation matrices [53] are employed to describe the position of the end effector of the manipulator in Equations 18 and 19.

$$\mathbf{H}_{i+1}^{i} = \begin{bmatrix} \mathbf{R}_{i+1}^{i} & \mathbf{P}_{i+1}^{i} \\ 0_{1\times3} & 1 \end{bmatrix} \tag{18}$$

$$\begin{bmatrix} \mathbf{P}_{i+1}^{base} \\ 1 \end{bmatrix} = \prod_{j=1}^{i} \mathbf{H}_{j+1}^{j} \times \begin{bmatrix} \mathbf{P}_{i+1}^{i} \\ 1 \end{bmatrix} \tag{19}$$

3.2.2   Inverse Kinematics

4 Result and Discussion

This is the Result and Discussion of the final report.

4.1 part ??

unknown

4.2 part ??

unknown

4.3 part ??

unknown

4.4 part ??

unknown

4.5 part ??

unknown

4.6 part ??

unknown

4.7 part ??

unknown

4.8 part ??

unknown

4.9   part ??

unknown

4.10   part ??

unknown

4.11   part ??

unknown

5   Conclusion

This is the Conclusion of the final report.

References

[1] Sarthak Misra, K. T. Ramesh, and Allison M. Okamura. Modeling of tool-tissue interactions for computer-based surgical simulation: A literature review. *Presence*, 17(5):463–491, 2008.

[2] Jessica Burgner-Kahrs, D. Caleb Rucker, and Howie Choset. Continuum robots for medical applications: A survey. *IEEE Transactions on Robotics*, 31(6):1261–1280, 2015.

[3] Pan Zhou, Jiantao Yao, Shuai Zhang, Chunjie Wei, Hongyu Zhang, and Shupeng Qi. A bioinspired fishbone continuum robot with rigid-flexible-soft coupling structure. *Bioinspiration & Biomimetics*, 17(6):066012, 2022.

[4] Jonathan M Sackier, Chuck Wooters, Lisa Jacobs, Amy Halverson, Darrin Uecker, and Yulun Wang. Voice activation of a surgical robotic assistant. *The American Journal of Surgery*, 174(4):406–409, 1997.

[5] Satyam Kalan, Sanket Chauhan, Rafael F Coelho, Marcelo A Orvieto, Ignacio R Camacho, Kenneth J Palmer, and Vipul R Patel. History of robotic surgery. *Journal of Robotic Surgery*, 4:141–147, 2010.

[6] TOMMASO FALCONE, JEFFREY GOLDBERG, Antonio Garcia-Ruiz, HAROUT MARGOSSIAN, and LAUREL STEVENS. Full robotic assistance for laparoscopic tubal anastomosis: a case report. *Journal of Laparoendoscopic & Advanced Surgical Techniques*, 9(1):107–113, 1999.

[7] Hermann Reichenspurner, Ralph J Damiano, Michael Mack, Dieter H Boehm, Helmut Gulbins, Christian Detter, Bruno Meiser, Reinhard Ellgass, and Bruno Reichart. Use of the voice-controlled and computer-assisted surgical system zeus

for endoscopic coronary artery bypass grafting. *The Journal of thoracic and cardiovascular surgery*, 118(1):11–16, 1999.

[8] Bertrand Guillonneau, Olivier Cappèle, Juan Bosco Martinez, Stèphane Navarra, and Guy Vallancien. Robotic assisted, laparoscopic pelvic lymph node dissection in humans. *The journal of urology*, 165(4):1078–1081, 2001.

[9] F. Pugin, P. Bucher, and P. Morel. History of robotic surgery : From aesop® and zeus® to da vinci®. *Journal of Visceral Surgery*, 148(5, Supplement):e3–e8, 2011. Robotic surgery.

[10] Chih Yu An, Jia Hao Syu, Ching Shiow Tseng, Chih-Ju Chang, et al. An ultrasound imaging-guided robotic hifu ablation experimental system and accuracy evaluations. *Applied Bionics and Biomechanics*, 2017, 2017.

[11] Sunita Chauhan, Hagey Amir, Guang Chen, Axel Hacker, Maurice Stephan Michel, and Kai Uwe Koehrmann. Intra-operative feedback and dynamic compensation for image-guided robotic focal ultrasound surgery. *Computer Aided Surgery*, 13(6):353–368, 2008.

[12] Sunita Chauhan. A mechatronic system for non invasive treatment of the breast cancers. In *Mechatronics and Machine Vision: John Billingsly (Eds)*. Research Studies Press Ltd, 2002.

[13] Sunita Chauhan, Ming Yeong Teo, and Wendy Teo. Robotic system for ablation of deep-seated skull base cancers—a feasibility study. In *Proceedings of the 34th International MATADOR Conference: Formerly The International Machine Tool Design and Conferences*, pages 21–27. Springer, 2004.

[14] Mohamed K Almekkaway, Islam A Shehata, and Emad S Ebbini. Anatomical-based model for simulation of hifu-induced lesions in atherosclerotic plaques. *International Journal of Hyperthermia*, 31(4):433–442, 2015.

[15] Laure-Anaïs Chanel, Florent Nageotte, Jonathan Vappou, Jianwen Luo, Loïc Cuvillon, and Michel de Mathelin. Robotized high intensity focused ultrasound (hifu) system for treatment of mobile organs using motion tracking by ultrasound imaging: An in vitro study. In *2015 37th Annual International Conference of*

the *IEEE Engineering in Medicine and Biology Society (EMBC)*, pages 2571–2575. IEEE, 2015.

[16] Andrea Cafarelli, Marco Mura, Alessandro Diodato, Andrea Schiappacasse, Matteo Santoro, Gastone Ciuti, and Arianna Menciassi. A computer-assisted robotic platform for focused ultrasound surgery: Assessment of high intensity focused ultrasound delivery. In *2015 37th Annual International Conference of the IEEE Engineering in Medicine and Biology Society (EMBC)*, pages 1311–1314. IEEE, 2015.

[17] Mark W Spong, Seth Hutchinson, and Mathukumalli Vidyasagar. *Robot modeling and control.* John Wiley & Sons, 2020.

[18] Michael E Moran. Evolution of robotic arms. *Journal of robotic surgery*, 1(2):103–111, 2007.

[19] Mark E Rosheim. *Robot evolution: the development of anthrobotics.* John Wiley & Sons, 1994.

[20] Bhaskar Dasgupta and TS1739334 Mruthyunjaya. The stewart platform manipulator: a review. *Mechanism and machine theory*, 35(1):15–40, 2000.

[21] Ray L Page. Brief history of flight simulation. *SimTecT 2000 proceedings*, pages 11–17, 2000.

[22] Roger Bostelman, James Albus, Nicholas Dagalakis, Adam Jacoff, John Gross, et al. Applications of the nist robocrane. In *Proceedings of the 5th International Symposium on Robotics and Manufacturing*, volume 5, page 1, 1994.

[23] Anastasia Puzatova, Pshtiwan Shakor, Vittoria Laghi, and Maria Dmitrieva. Large-scale 3d printing for construction application by means of robotic arm and gantry 3d printer: A review. *Buildings*, 12(11):2023, 2022.

[24] Byung-In Kim, Sunderesh S Heragu, Robert J Graves, and Art St Onge. Clustering-based order-picking sequence algorithm for an automated warehouse. *International Journal of Production Research*, 41(15):3445–3460, 2003.

[25] Ishak WI Wan, WH Kit, and MA Awal. Design and development of eggplant harvester for gantry system. *Pertanika Journal of Science & Technology*, 18(2), 2010.

[26] Eberhard Abele, Matthias Weigold, and Stefan Rothenbücher. Modeling and identification of an industrial robot for machining applications. *CIRP annals*, 56(1):387–390, 2007.

[27] Shin-ichi Matsuoka, Kazunori Shimizu, Nobuyuki Yamazaki, and Yoshinari Oki. High-speed end milling of an articulated robot and its characteristics. *Journal of materials processing technology*, 95(1-3):83–89, 1999.

[28] Hoai Nam Huynh, Hamed Assadi, Edouard Rivière-Lorphèvre, Olivier Verlinden, and Keivan Ahmadi. Modelling the dynamics of industrial robots for milling operations. *Robotics and Computer-Integrated Manufacturing*, 61:101852, 2020.

[29] See Han Tay, Wai Heng Choong, and Hou Pin Yoong. A review of scara robot control system. In *2022 IEEE International Conference on Artificial Intelligence in Engineering and Technology (IICAIET)*, pages 1–6, 2022.

[30] Rishabh Chaturvedi, Anas Islam, and Kamal Sharma. Anticipated investigation of a cylindrical robot arm by means of compound materials. *Eur J Mol Clin Med*, 7(4):736–745, 2020.

[31] Foster Collins and Mark Yim. Design of a spherical robot arm with the spiral zipper prismatic joint. In *2016 IEEE international conference on robotics and automation (ICRA)*, pages 2137–2143. IEEE, 2016.

[32] Varnita Verma, A Gupta, MK Gupta, and P Chauhan. Performance estimation of computed torque control for surgical robot application. *Journal of Mechanical Engineering and Sciences*, 14(3):7017–7028, 2020.

[33] Erhan Akdoğan and Mehmet Arif Adli. The design and control of a therapeutic exercise robot for lower limb rehabilitation: Physiotherabot. *Mechatronics*, 21(3):509–522, 2011.

[34] Lu Zongxing, Li Wanxin, and Zhang Liping. Research development of soft manipulator: A review. *Advances in Mechanical Engineering*, 12(8):1687814020950094, 2020.

[35] Deepak Trivedi, Christopher D Rahn, William M Kier, and Ian D Walker. Soft robotics: Biological inspiration, state of the art, and future research. *Applied bionics and biomechanics*, 5(3):99–117, 2008.

[36] Cecilia Laschi, Barbara Mazzolai, Virgilio Mattoli, Matteo Cianchetti, and Paolo Dario. Design of a biomimetic robotic octopus arm. *Bioinspiration & biomimetics*, 4(1):015006, 2009.

[37] Michael W Hannan and Ian D Walker. Kinematics and the implementation of an elephant's trunk manipulator and other continuum style robots. *Journal of robotic systems*, 20(2):45–63, 2003.

[38] Cecilia Laschi, Matteo Cianchetti, Barbara Mazzolai, Laura Margheri, Maurizio Follador, and Paolo Dario. Soft robot arm inspired by the octopus. *Advanced robotics*, 26(7):709–727, 2012.

[39] Fionnuala Connolly, Conor J Walsh, and Katia Bertoldi. Automatic design of fiber-reinforced soft actuators for trajectory matching. *Proceedings of the National Academy of Sciences*, 114(1):51–56, 2017.

[40] Shujun Wei, Tianyu Wang, and Guoving Gu. Design of a soft pneumatic robotic gripper based on fiber-reinforced actuator. *Journal of Mechanical Engineering*, 53(13):29–38, 2017.

[41] Bobak Mosadegh, Panagiotis Polygerinos, Christoph Keplinger, Sophia Wennstedt, Robert F Shepherd, Unmukt Gupta, Jongmin Shim, Katia Bertoldi, Conor J Walsh, and George M Whitesides. Pneumatic networks for soft robotics that actuate rapidly. *Advanced functional materials*, 24(15):2163–2170, 2014.

[42] Ramses V Martinez, Jamie L Branch, Carina R Fish, Lihua Jin, Robert F Shepherd, Rui Nunes, Zhigang Suo, and George McClelland Whitesides. Robotic tentacles with three-dimensional mobility based on flexible elastomers. *Advanced materials*, 2013.

[43] Run Wang, Nan Jiang, Jian Su, Qu Yin, Yue Zhang, Zhongsheng Liu, Haibao Lin, Francisco A Moura, Ningyi Yuan, Siegmar Roth, et al. A bi-sheath fiber sensor for giant tensile and torsional displacements. *Advanced Functional Materials*, 27(35):1702134, 2017.

[44] Eric Brown, Nicholas Rodenberg, John Amend, Annan Mozeika, Erik Steltz, Mitchell R Zakin, Hod Lipson, and Heinrich M Jaeger. Universal robotic gripper based on the jamming of granular material. *Proceedings of the National Academy of Sciences*, 107(44):18809–18814, 2010.

[45] Caleb Christianson, Nathaniel N Goldberg, Dimitri D Deheyn, Shengqiang Cai, and Michael T Tolley. Translucent soft robots driven by frameless fluid electrode dielectric elastomer actuators. *Science Robotics*, 3(17):eaat1893, 2018.

[46] QM Zhang, Hengfeng Li, Martin Poh, Feng Xia, Z-Y Cheng, Haisheng Xu, and Cheng Huang. An all-organic composite actuator material with a high dielectric constant. *Nature*, 419(6904):284–287, 2002.

[47] Bertrand Tondu, Serge Ippolito, Jérémie Guiochet, and Alain Daidie. A seven-degrees-of-freedom robot-arm driven by pneumatic artificial muscles for humanoid robots. *The International Journal of Robotics Research*, 24(4):257–274, 2005.

[48] David Jakes, Zongyuan Ge, and Liao Wu. Model-less active compliance for continuum robots using recurrent neural networks. In *2019 IEEE/RSJ International Conference on Intelligent Robots and Systems (IROS)*, pages 2167–2173. IEEE, 2019.

[49] Ernar Amanov, Thien-Dang Nguyen, and Jessica Burgner-Kahrs. Tendon-driven continuum robots with extensible sections—a model-based evaluation of path-following motions. *The International Journal of Robotics Research*, 40(1):7–23, 2021.

[50] Ammar Amouri, Abdelhakim Cherfia, Ayman Belkhiri, and Halim Merabti. Bio-inspired a novel dual-cross-module sections cable-driven continuum robot: design, kinematics modeling and workspace analysis. *Journal of the Brazilian Society of Mechanical Sciences and Engineering*, 45(5):265, 2023.

[51] Tomer Anor, Joseph R. Madsen, and Pierre Dupont. Algorithms for design of continuum robots using the concentric tubes approach: A neurosurgical example.

In *2011 IEEE International Conference on Robotics and Automation*, pages 667–673, 2011.

[52] Priyanka Rao, Quentin Peyron, Sven Lilge, and Jessica Burgner-Kahrs. How to model tendon-driven continuum robots and benchmark modelling performance. *Frontiers in Robotics and AI*, 7:630245, 2021.

[53] Sébastien Briot, Wisama Khalil, Sébastien Briot, and Wisama Khalil. Homogeneous transformation matrix. *Dynamics of Parallel Robots: From Rigid Bodies to Flexible Elements*, pages 19–32, 2015.

Appendix A

TEST

This is the Appendix 1.

Appendix B

Test

This is the Appendix 2.